Deformation fabrics of natural blueschists and implications for seismic anisotropy in subducting oceanic crust

CrossMark

Daeyeong Kim [a,*], Ikuo Katayama [a], Katsuyoshi Michibayashi [b], Tatsuki Tsujimori [c]

[a] Department of Earth and Planetary Systems Science, Graduate School of Science, Hiroshima University, Higashi-Hiroshima 739-8526, Japan
[b] Institute of Geosciences, Shizuoka University, Shizuoka 422-8529, Japan
[c] Pheasant Memorial Laboratory, Institute for Study of the Earth's Interior, Okayama University, Misasa, Tottori 682-0193, Japan

ABSTRACT

Investigations of microstructures are crucial if we are to understand the seismic anisotropy of subducting oceanic crust, and here we report on our systematic fabric analyses of glaucophane, lawsonite, and epidote in naturally deformed blueschists from the Diablo Range and Franciscan Complex in California, and the Hida Mountains in Japan. Glaucophanes in the analyzed samples consist of very fine grains that are well aligned along the foliation and have high aspect ratios and strong crystal preferred orientations (CPOs) characterized by a (1 0 0)[0 0 1] pattern. These characteristics, together with a bimodal distribution of grain sizes from some samples, *possibly* indicate the occurrence of dynamic recrystallization for glaucophane. Although lawsonite and epidote display high aspect ratios and a strong CPO of (0 0 1)[0 1 0], the occurrence of straight grain boundaries and euhedral crystals indicates that rigid body rotation was the dominant deformation mechanism. The P-wave (AV_P) and S-wave (AV_S) seismic anisotropies of glaucophane ($AV_P = 20.4\%$, $AV_S = 11.5\%$) and epidote ($AV_P = 9.0\%$, $AV_S = 8.0\%$) are typical of the crust; consequently, the fastest propagation of P-waves is parallel to the [0 0 1] maxima, and the polarization of S-waves parallel to the foliation can form a trench-parallel seismic anisotropy owing to the slowest V_S polarization being normal to the subducting slab. The seismic anisotropy of lawsonite ($AV_P = 9.6\%$, $AV_S = 19.9\%$) is characterized by the fast propagation of P-waves subnormal to the lawsonite [0 0 1] maxima and polarization of S-waves perpendicular to the foliation and lineation, which can generate a trench-normal anisotropy. The AV_S of lawsonite blueschist (5.6–9.2%) is weak compared with that of epidote blueschist (8.4–11.1%). Calculations of the thickness of the anisotropic layer indicate that glaucophane and lawsonite contribute to the trench-parallel and trench-normal seismic anisotropy beneath NE Japan, but not to that beneath the Ryukyu arc. Our results demonstrate, therefore, that lawsonite has a strong influence on seismic velocities in the oceanic crust, and that lawsonite might be the cause of complex anisotropic patterns in subduction zones.

© 2013 Elsevier B.V. All rights reserved.

1. Introduction

The propagation of seismic waves is a powerful tool for understanding the rheological behavior of the Earth at depth. In subduction zones, seismic properties can provide information about the origin of the slab, the nature of the mantle wedge, slab rollback, and help us to understand back-arc spreading and to detect the presence of melts (e.g., Wines et al., 2008). In particular, trench-parallel and trench-perpendicular shear-waves are observed in subduction zones from the polarization directions of fast propagations and the delay time between the arrivals of fast and slow shear-waves. These shear waves have been explained by theories that involve the flow of the mantle (Long and Silver, 2008) or the

crystal preferred orientations (CPOs) of minerals such as olivine (Jung and Karato, 2001) and serpentine (Katayama et al., 2009). The precise source of the seismic anisotropy in subduction zones, however, is not well defined by the shear-wave splitting method, and further studies of the mantle wedge and the subducting slab are therefore essential. In addition, recent studies have emphasized the importance of minerals such as glaucophane and lawsonite in blueschists for explaining the low velocity layer (LVL) (Chantel et al., 2012; Mookherjee and Bezacier, 2012).

The decrease of seismicity in the upper seismic zone of subducting oceanic crust might be related to a change in rock type from blueschist to eclogite (Kita et al., 2006), signifying the importance of rock-forming minerals in explaining the seismic properties. Glaucophane, lawsonite, and epidote are characterized by high water contents (~2.0–2.5 wt% for glaucophane, l.0–11.5 wt% for lawsonite, and 1.95 wt% for epidote) and strong P-wave (AV_P) and

* Corresponding author. Tel.: +81 80 1635 5435.
  E-mail address: daeyeongkim@hiroshima-u.ac.jp (D. Kim).

S-wave (AV_S) seismic anisotropies in single crystals ($AV_P = 38.1\%$ and $AV_S = 27.3\%$ for glaucophane, $AV_P = 74\%$ for lawsonite, and $AV_S = 21\%$ for epidote; Schmidt and Poli, 1998; Sinogeikin et al., 2000; Mao et al., 2007; Bezacier et al., 2010). In addition, previous studies have noted variations in seismic anisotropy, possibly caused by glaucophane CPOs in combination with a diverse range of lawsonite and epidote CPOs (Bezacier et al., 2010; Fujimoto et al., 2010; Teyssier et al., 2010).

In this paper we record the results of fabric analyses of several lawsonite and epidote blueschists from the New Idria serpentinite body of the Diablo Range and Ward Creek, Cazadero, California, USA, and the Omi serpentinite mélange of the Hida Mountains in Japan. We have assessed the deformational behavior of glaucophane, lawsonite, epidote, and the blueschists on the basis of microstructures, aspect ratios, and CPOs relative to foliation, and their seismic properties have been calculated. Additionally, we discuss the tectonic implications of these three minerals with respect to seismic velocities and anisotropic patterns in a subduction zone.

2. Sample localities

2.1. The New Idria serpentinite body, Diablo Range, California

Located between the San Andreas Fault on the west and the San Joaquin Valley on the east, the New Idria serpentinite body in the Diablo Range is exposed along the crest of the Coalinga anticline, and is enclosed by high-angle normal faults that denote the exhumed trace of the Coast Range Fault (Coleman, 1980). The New Idria serpentinite is primarily chrysotile–lizardite, with minor antigorite serpentinite, and it represents the retrogression of a moderately depleted harzburgite that contained numerous tectonic blocks of greenstone and low-grade blueschists (Coleman, 1980; Tsujimori et al., 2007). A sample of highly deformed lawsonite blueschist (sample NI-01) was collected at a nearby eclogite locality where retrograde eclogite and garnet amphibolite, originating from mantle depths, are exposed along Clear Creek (Table 1) (Tsujimori et al., 2007; Kim et al., 2013). The data in this paper on the rheological contrasts of glaucophane and lawsonite have already been reported (Kim et al., 2013). We found it necessary to use these same data in this paper for our calculations of seismic anisotropies of the subducting oceanic crust, because such highly foliated lawsonite blueschists occur very rarely.

2.2. The Ward Creek schist, Franciscan Complex, California

The Ward Creek schist, represented by metamorphosed oceanic basalts and overlying pelagic sediments, occurs within the Franciscan Complex in the central belt of the northern Coast Ranges of California, and lies within type-III blueschists (Coleman and Lee, 1963; Maruyama and Liou, 1987, 1988). The type-III rocks are characterized by a well-developed schistosity, a fine grain size, and a banded structure with layers composed mainly of metamorphosed basalts, cherts, shales, ironstones, and carbonates. We selected and collected a highly foliated garnet-bearing blueschist (CZ-02) close to the lawsonite eclogite locality (Table 1) (Tsujimori et al., 2006).

2.3. The Omi serpentinite mélange, Hida Mountains, Japan

The Renge schist, an older geotectonic unit in the Sangun metamorphic belt, considered to be one of the higher-pressure schists in Japan, mainly comprises metasediments such as pelitic, psammitic and siliceous schists, and metabasites with minor metagabbro. The glaucophane schist in the Omi area, located at the northern end of the Hida Mountains, occurs in the southern chlorite zone of the Renge schist (Banno, 1958; Tsujimori et al., 2000). The glaucophane-bearing metabasites are locally intercalated with micaceous schist in a fault-bounded eclogitic unit that corresponds to the southern chlorite zone. The analyzed samples (Omi-02 and 03) were collected in areas of garnet glaucophane schist and epidote glaucophane schist (Table 1).

3. Analytical techniques

The chemical compositions of the amphiboles were determined by electron probe microanalysis (EPMA, JEOL JXA-8200) at Hiroshima University, Japan. The analytical conditions were as follows: accelerating voltage of 15 kV, beam current of 10 nA, and spot size of 3–5 μm with Kα lines for Si, Ti, Al, Cr, Fe, Mn, Mg, Ca, Na, and K. The Fe^{3+} contents in the amphiboles were calculated as the average of the maximum and minimum estimates based on a total of 13 cations for T and C sites and 15 cations for T, C, and B sites (Leake et al., 1997).

Image analyses in sections parallel to the lineation and normal to the foliation were made in order to quantify the aspect ratios of mineral grains, and to determine the angles between the longest

Table 1
Sample locations and the results of fabric analysis.

Sample numbers	Location (lattitude, longitude)	Lithology	Mode* (%)	Minerals	Grain size with std. dev. (μm)	Aspect ratio with std. dev.	Fabric strength (CPO)		Seismic anisotropy (%)	
							Number	J	AV_P	AV_S
GRL_NI-01	36°38′, −120°71′	Lawsonite blueschist	Gln89, Lws8	Gln	7 ± 3	12.8 ± 6.4	218	18.0	25.3	13.9
				Lws	18 ± 6	5.0 ± 2.3	220	9.6	10.7	21.3
LRL_NI-01	36°38′, −120°71′	Lawsonite blueschist	Gln64, Lws21	Gln	12 ± 5	6.0 ± 2.8	220	16.0	20.2	9.9
				Lws	20 ± 8	3.6 ± 1.5	219	7.8	8.8	19.4
CZ-02	36°54′, −123°11′	Grt-bearing lawsonite blueschist	Gln81, Cpx8, Grt4	Gln	59 ± 29	5.2 ± 2.3	253	9.8	17.7	8.4
Omi-02	36°85′, 137°74′	Grt-bearing epidote blueschist	Gln54, Ep27, Ttn10, Grt5	Gln	18 ± 7	3.0 ± 1.4	261	9.0	19.5	10.4
				Ep	18 ± 7	2.1 ± 0.6	241	7.2	7.1	5.6
GRL_Omi-03	36°81′, 137°74′	Epidote blueschist	Gln91, Ep6	Gln	6 ± 3	3.5 ± 1.6	260	32.5	29.5	18.4
				Ep	10 ± 6	3.4 ± 1.4	231	12.5	11.1	11.9
ERL_Omi-03	36°81′, 137°75′	Epidote blueschist	Ep57, Gln20, Ph19	Gln	9 ± 6	3.0 ± 1.6	247	19.2	27.5	16.6
				Ep	17 ± 10	2.8 ± 1.1	248	8.8	9.7	8.5

Mode* excludes phengite, titanite and apatite (abundances of each mineral are less than 5%). Gln: glaucophane; Lws: lawsonite, Cpx: clinopyroxene; Grt: garnet; Ttn: titanite; Ep: epidote; Ph: phengite; Number: number of measurements; J: J-index, respectively.

axes of various grains and the foliation. After tracing grain boundaries, best-fit ellipses (calculated using ImageJ 1.44) were adopted to reduce the complexity of the various shapes of grains (e.g., Mezger, 2010; Kim et al., 2013). Grain sizes were calculated as the area of a square with the same internal area as the calculated best-fit ellipse.

Crystallographic preferred orientations of glaucophane, lawsonite, and epidote were measured by indexation of electron backscattered diffraction (EBSD) patterns (Randle, 1992; Prior et al., 1999; Randle and Engler, 2000) using an Oxford–HKL–EBSD on a Hitachi S-3400 scanning electron microscope (SEM) at Shizuoka University, Japan. The CPO measurements were conducted with an accelerating voltage of 20 kV, a working distance of 28 mm, and a beam current of ca. 10 nA. Automatic mapping of each sample (1 μm step size) was performed to examine the chemical zoning in glaucophane, lawsonite, and epidote. After we confirmed that an identical lattice orientation accompanied the chemical variations, the EBSD patterns were manually indexed by considering single individual points for each grain. The number of analysis points was standardized at 240 ± 22 to ensure the reliability of data and to allow for comparison among samples. Pole figures were plotted using the software PFch5 written by D. Mainprice, and the fabric strength was determined by the J-index (Bunge, 1982; Mainprice and Silver, 1993).

The seismic properties of glaucophane, lawsonite, epidote, and whole rocks made up of those minerals were calculated in order to understand their influence on the seismic properties of the subducting oceanic crust. The P-wave seismic anisotropy (AV_P) is normally described as the difference between the maximum and minimum velocities in two dissimilar propagating paths, and ex-

pressed as a percentage. For example, the AV_{Pmax} can be estimated by using the formula $200 (V_{Pmax} - V_{Pmin})/(V_{Pmax} + V_{Pmin})$. The S-wave seismic anisotropy (AV_S) is defined as the difference between two dissimilar velocities of two orthogonally polarized S-waves individually propagating through an anisotropic medium. Hence, the percentage AV_{Smax} is evaluated using the formula $200 (V_{S1} - V_{S2})/(V_{S1} + V_{S2})$, in which V_{S1} and V_{S2} are the fast and slow velocities, respectively. In this study, the calculations of whole rock seismic properties were made with reference to the modal abundances of each mineral (Table 1) (Mainprice, 1990; Mainprice et al., 2000). We employed the respective single crystal elastic constants (C_{ij}) of glaucophane (Bezacier et al., 2010), lawsonite (Sinogeikin et al., 2000), and epidote (Aleksandrov et al., 1974), and their densities with the Voigt–Reuss–Hill averaging scheme.

4. Description of microstructures and chemical compositions of amphibole

The sample from the New Idria serpentinite body is a fine-grained blueschist mostly composed of glaucophane, lawsonite, titanite, and phengite. It contains two distinct layers: (i) glaucophane-rich layers (GRL NI-01) and (ii) lawsonite-rich layers (LRL NI-01) (Figs. 1a, b and 2a, b; Table 1). Very fine-grained GRL NI-01 shows highly foliated microstructures with low contents of phengite. Anhedral glaucophane has grain size ranging from ~1 to ~15 μm, irregular grain boundaries, and undulose extinction. Lawsonite is subhedral or euhedral and displays small grain size between ~10 and ~30 μm. Relatively fine-grained LRL NI-01 is characterized by relatively large grains of lawsonite with significant amounts of phengite around them (Figs. 1b and 2b). Intersti-
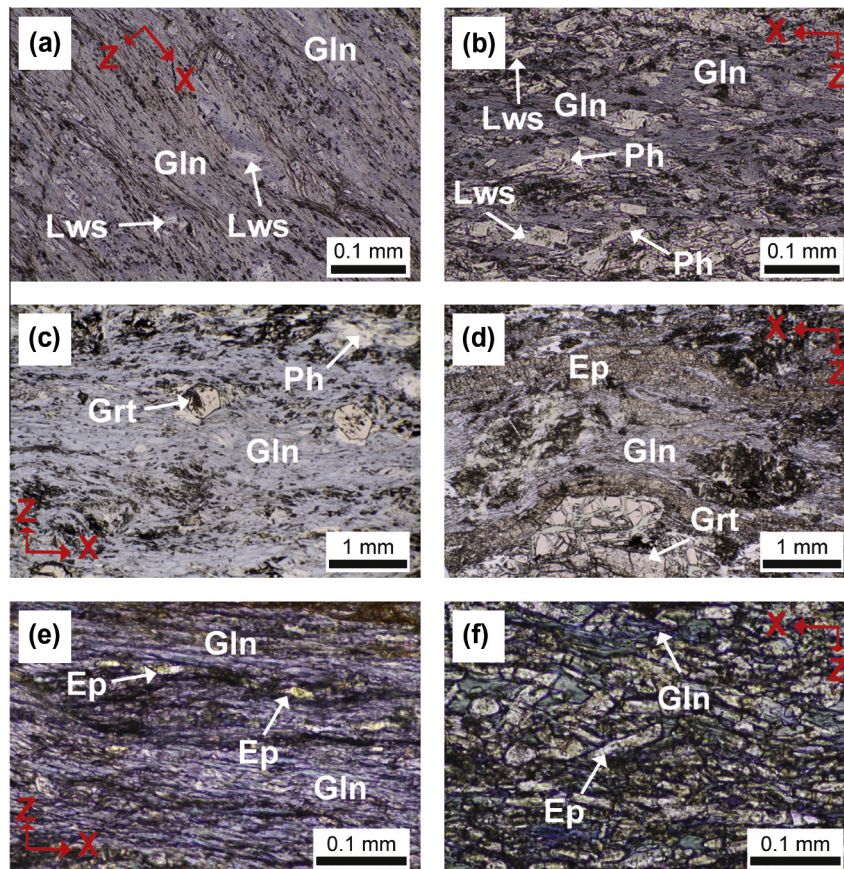
Fig. 1. Photomicrographs of the analyzed samples (XZ sections). (a) Glaucophane-rich and (b) lawsonite-rich layers in NI-01 collected from the New Idria serpentinite body, Diablo Range, California. (c) CZ-02 from Ward Creek, Franciscan Complex, California. (d) Omi-02 and (e) glaucophane-rich and (f) epidote-rich layers in Omi-03 from the Omi serpentinite mélange, Hida Mountains, Japan. See Table 1 for sample locations. Mineral abbreviations follow those in Whitney and Evans (2010).
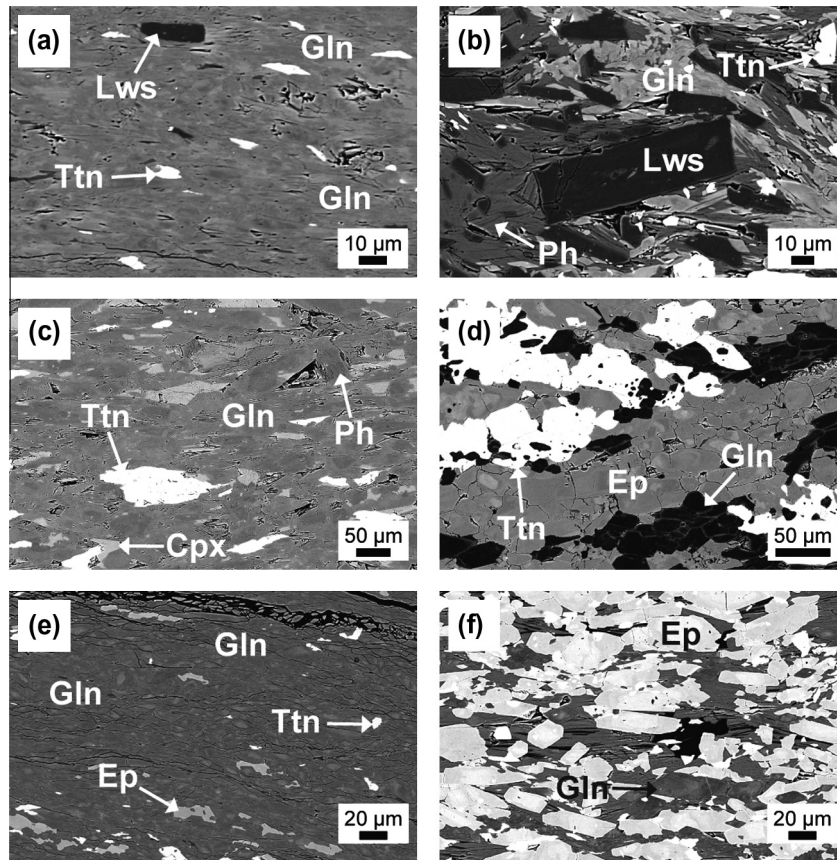
Fig. 2. Backscattered electron images of the analyzed samples (XZ sections: X, horizontal; Z, vertical). (a) Glaucophane-rich and (b) lawsonite-rich layers in NI-01. (c) CZ-02. (d) Omi-02. (e) Glaucophane-rich and (f) epidote-rich layers in Omi-03. Mineral abbreviations follow those in Whitney and Evans (2010).

tial glaucophane is relatively fine-grained (~5 to ~20 μm) and anhedral to subhedral. Porphyroclastic lawsonite has angular and straight grain boundaries, euhedral grain shape, and grain size ranging from ~10 to ~30 μm, and weakens the overall shape preferred orientation (Fig. 2).

The highly foliated Ward Creek lawsonite blueschist (CZ-02) is characterized by prograde-zoned garnet and relatively large grains (~30 to ~100 μm) of subhedral glaucophane (Figs. 1c and 2c). Fine-grained (~10 μm) garnet grains are mostly euhedral or subhedral and sometimes have a reaction texture with clinopyroxene and white mica. Although the sections used in this study contain only small amounts of lawsonite (<2%), the mineral assemblage garnet + lawsonite nevertheless represents the peak metamorphic conditions.

The Omi epidote blueschists (Omi-02 and 03) have a relatively weak foliation and lineation (Fig. 1d, e, and f). The garnet-bearing epidote blueschist (Omi-02) predominantly comprises glaucophane and epidote. Large grained (>1 mm) garnet is usually broken and the area between grains is filled by clinopyroxene. Fine-grained glaucophane (~5 to ~10 μm) and epidote (~5 to ~10 μm) generally have smooth grain boundaries, which might have been affected by grain boundary area reduction during the main deformation event (Fig. 2d). Most glaucophanes have a weak chemical zoning. The specimen Omi-03 from the area of epidote glaucophane schist (Tsujimori, 2002) can be divided into glaucophane-rich (GRL Omi-03) and epidote-rich (ERL Omi-03) layers (Fig. 1e and f) by a similar criterion with the NI-01. The GRL Omi-03 is a very fine-grained blueschist. Highly foliated glaucophane has irregular grain boundaries, undulose extinction, and very fine grains (<~10 μm), and epidote displays anhedral to subhedral grain shape with size ranging from ~5 to ~20 μm. The ERL

Omi-03 is characterized by relatively large and euhedral epidote (~10 to ~30 μm) with interstitial glaucophane (~5 to ~20 μm). Sometimes chemical zoning can be observed for glaucophane.

Glaucophane, a sodic amphibole, is defined by $(Na + K)_A < 0.50$, $Mg/(Mg + Fe^{2+}) \geqslant 0.5$, and $^6Al \geqslant Fe^{3+}$ (Leake et al., 1997). Therefore, most of the spots we analyzed can be defined as glaucophane (Fig. 3; Table 2). A few spots located in the cores or rims of glaucophane plot instead as magnesioriebeckite, winchite, or actinolite (Fig. 3). Our analyzed glaucophanes are characterized by a decrease in Al from core to rim (Table 2), suggesting they formed during retrogression (Maruyama et al., 1986). The mineral assemblages (and making due reference to previous studies of similar assemblages) indicate peak metamorphic conditions of $P > 1.0$ GPa and $T = 200–290 °C$ for the New Idria lawsonite blueschists, $P \sim 1.8–2.2$ GPa and $T = 430–440 °C$ for the Ward Creek lawsonite blueschists, and ~1 GPa and 400–460 °C for the Omi epidote blueschists (Maruyama and Liou, 1988; Tsujimori, 2002; Tsujimori et al., 2006, 2007). Although an increase in Al from core to rim could be observed in GRL Omi-03 (Table 2), the glaucophane in the matrix would normally have formed by the retrograde metamorphism of eclogite and by the alteration of jadeite (Deer et al., 1992). In addition, Tsujimori (2002) reported that retrograde blueschist-facies overprinting is in garnet-free P–T range. We have therefore adopted the metamorphic conditions noted above for this study.

5. Results

5.1. Microscopic analyses

Most of the glaucophane has a high aspect ratio (3.0–12.8) with long axes at low angles to the foliation (Fig. 4; Table 1). In the New
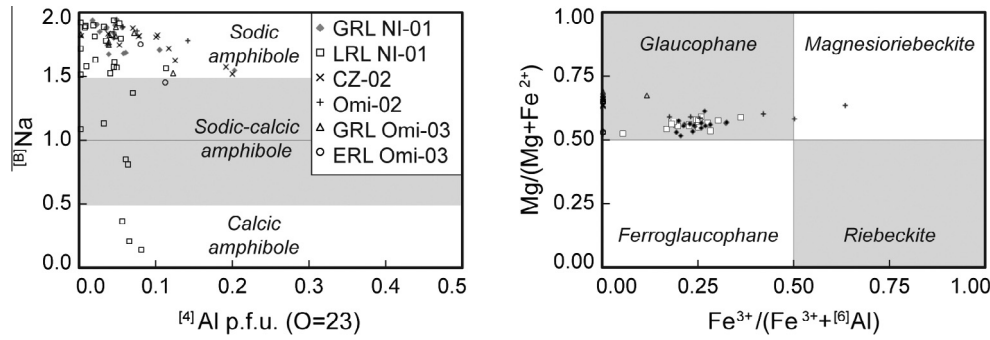
Fig. 3. Chemical compositions of the amphiboles. Ferric iron was calculated from the average of the maxima and minima estimated according to a total of 15 cations at T, C, and B sites, and 13 cations at T and C sites (Leake et al., 1997).

Table 2
Chemical compositions of representative sodic amphiboles in each sample.

Sample No.	NI-01				CZ-02		Omi-02		Omi-03			
Area	Glaucophane-rich layer		Lawsonite-rich layer						Glaucophane-rich layer		Epidote-rich layer	
Spot No.	110408-8	110408-10	110401-50C	110401-51R	120419-51C	120419-47R	120419-26	120419-21	120419-01C	120419-02R	120419-12C	120419-11R
SiO$_2$	55.39	53.53	56.33	56.35	57.41	56.84	57.46	56.84	55.44	56.21	55.87	54.33
TiO$_2$	0.04	0.02	0.10	–	0.04	0.01	–	–	0.07	–	0.06	0.05
Al$_2$O$_3$	7.11	8.73	8.62	7.84	11.52	10.33	11.22	11.19	3.60	8.43	8.36	5.82
Cr$_2$O$_3$	0.03	0.02	0.02	0.03	0.04	0.04	–	0.03	0.02	0.03	0.01	0.02
FeO*	16.40	16.04	15.09	14.94	9.18	10.28	10.18	10.18	19.33	14.99	15.16	16.34
MnO	0.16	0.24	0.07	0.21	0.09	0.19	0.03	0.02	0.13	0.16	0.17	0.19
MgO	8.63	9.05	8.54	9.18	10.44	10.43	9.99	9.83	9.81	8.79	9.18	10.00
CaO	1.27	1.29	0.41	2.28	1.08	1.32	0.68	0.96	0.59	0.65	1.10	3.12
Na$_2$O	6.92	6.32	7.51	6.15	7.06	6.66	7.31	7.20	7.10	7.32	6.85	5.80
K$_2$O	0.01	0.02	0.02	0.03	0.02	0.01	–	–	–	0.01	0.01	0.03
Total	95.95	95.24	96.71	97.00	96.87	96.11	96.87	96.23	96.08	96.59	96.76	95.69
Cations	*O = 23*	*O = 23*	*O = 23*	*O = 23*	*O = 23*	*O = 23*	*O = 23*	*O = 23*	*O = 23*	*O = 23*	*O = 23*	*O = 23*
Si	7.96	7.80	7.96	7.98	7.92	7.95	7.94	7.93	8.00	7.95	7.92	7.89
Ti	0.00	0.00	0.01	–	0.00	0.00	–	–	0.01	–	0.01	0.01
Al	1.20	1.50	1.44	1.31	1.88	1.70	1.83	1.84	0.61	1.41	1.40	1.00
Cr	0.00	0.00	0.00	0.00	0.00	0.00	–	0.00	0.00	0.00	0.00	0.00
Fe^{3+}	0.54	0.46	0.46	0.29	0.00	0.00	0.00	0.17	1.04	0.46	0.00	0.00
Fe^{2+}	1.43	1.49	1.32	1.48	1.06	1.20	1.18	1.02	1.30	1.32	1.80	1.98
Mn	0.02	0.03	0.01	0.03	0.01	0.02	0.00	0.00	0.02	0.02	0.02	0.02
Mg	1.85	1.97	1.80	1.94	2.15	2.18	2.06	2.04	2.11	1.85	1.94	2.17
Ca	0.20	0.20	0.61	0.35	0.16	0.20	0.10	0.14	0.09	0.10	0.17	0.49
Na	1.93	1.79	2.06	1.69	1.89	1.81	1.96	1.86	1.99	2.01	1.88	1.63
K	0.00	0.00	0.00	0.01	0.00	0.00	–	–	0.16	0.12	0.00	0.01
Total	15.13	15.24	15.67	15.07	15.08	15.06	15.07	15.00	15.32	15.23	15.14	15.19
gln	0.66	0.75	0.77	0.70	0.96	0.93	0.99	0.89	0.38	0.75	0.98	0.84
mrb	0.31	0.27	0.26	0.16	0.00	0.00	0.00	0.09	0.65	0.25	0.00	0.00
act	0.38	0.32	0.12	0.68	0.30	0.37	0.19	0.28	0.17	0.19	0.31	0.89
ts	0.00	0.01	0.00	0.00	0.00	0.00	0.00	0.00	0.00	0.00	0.00	0.01

C, core; R, rim; -, not detected. FeO* indicates total Fe as Fe^{2+}. The Fe^{3+} calculation of glaucophane employs the average of maximum and minimum values (Leake et al., 1997).

Idria blueschists, lawsonite has a relatively low aspect ratio (3.6–5.0) with long axes at higher angles to the foliation than glaucophane (Fig. 4a, b; Table 1). Epidote is characterized by grains of relatively low aspect ratio (2.1–3.4), with long axes at high angles to the foliation (Fig. 4d–f; Table 1).

Fig. 5 shows the grain size distributions in the analyzed samples. To deal with uncertainties and trivial peaks, we assume that points higher than a frequency of 5 are valid. Glaucophane typically displays a very fine grain size (1–59 μm), with two peaks in the grain size distributions for the New Idria blueschists, and a single peak for the Ward Creek and Omi blueschists (Fig. 5; Table 1). The lawsonite is characterized by slightly larger grains (15–20 μm) and a broader range of grain size (10–30 μm) with a single peak (Fig. 5; Table 1). Epidote usually has a fine grain size (10–20 μm)

with a single peak, except in the Omi-03 (Fig. 5; Table 1). The Omi-03 contains two certain peaks of grain size distributions of epidote. The grain size distribution data shows, therefore, that a single peak in the distributions is common, that two peaks could be observed for glaucophane in the New Idria blueschists and epidote in the Omi blueschists, and that glaucophane has the smallest grain size.

5.2. EBSD patterns

Glaucophane, lawsonite, and epidote each have distinctive CPOs. Pole figures of glaucophane in the analyzed samples have (100) subparallel to the foliation and [001] subparallel to the lineation (Fig. 6), with the *J*-index intensity ranging from 9.0 (Omi-02)
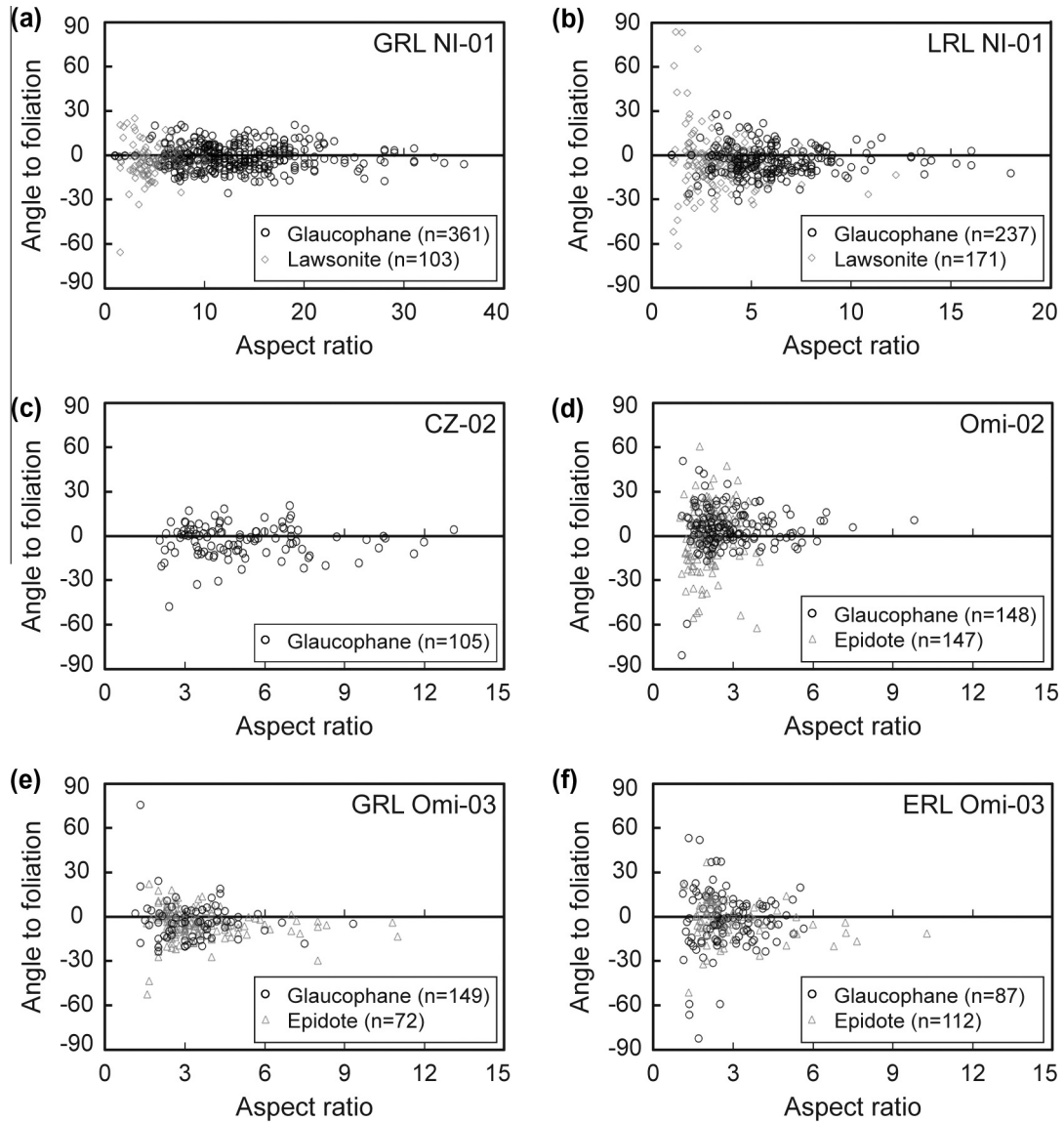
Fig. 4. Angles between grain long-axes and the mean foliation plane vs. aspect ratios, as calculated using the image-analysis software ImageJ 1.44 (http://rsb.info.nih.gov/ij/). Best-fit ellipses were used to reduce the complexity of diverse shapes.

to 32.5 (GRL Omi-03) (Table 1). Lawsonite in the New Idria blueschist (NI-01) has [010] subparallel to the lineation, foliation-subnormal [001] axes, and scattered [100] (Fig. 7). The J-index intensity for lawsonite in the New Idria blueschist (NI-01) is 7.8 in the GRL and 9.6 in the LRL (Table 1). Epidote has (010) subparallel to the lineation, [001] subnormal to the foliation, and (100) has a scattered distribution (Fig. 8). The value of the J-index intensity ranges from 7.2 (Omi-02) to 12.5 (GRL Omi-03) (Table 1). The (100) poles of glaucophane in the epidote blueschist (Omi-03) particularly have a higher *pfj* than [100] axes parallel to the lineation, suggesting the stronger development of a foliation rather than a lineation (Fig. 6). The J-indices of poles figures can be compared with the grain sizes of glaucophane, lawsonite, and epidote in Table 1 and the plots of Figs. 6–8.

5.3. Seismic anisotropy

The V_P, V_{S1}, V_{S2}, AV_S, and V_{S1} polarizations of average glaucophane, lawsonite, epidote, and whole rocks for the New Idria lawsonite blueschist (NI-01) and Omi epidote blueschist (Omi-03) are projected onto the lower hemisphere in Figs. 9 and 10. Since the number of analysis points for each sample is similar (240 ± 22), the average seismic properties can be calculated from the sum of data for each sample. The seismic properties of average glaucophane are estimated to be 6.87–8.42 km/s for V_P, 4.39–4.86 km/s for V_{S1}, and 4.32–4.54 km/s for V_{S2}, with a seismic anisotropy of 20.4% for AV_P and 11.48% for AV_S (Fig. 9a). The patterns for average glaucophane show V_{Pmax} along the lineation, AV_{Smax} and V_{S1max} polarization subparallel to the foliation, and with the directions of V_{Pmin}, AV_{Smin}, and V_{S1min} polarization normal to the foliation. The V_P value of average lawsonite is calculated to be 7.66–8.44 km/s, V_{S1} is 4.02–4.55 km/s, and V_{S2} is 3.69–4.24 km/s, with a strong seismic anisotropy ($AV_P = 9.6\%$, $AV_S = 19.88\%$) (Fig. 9b). The V_{Pmax} of average lawsonite is developed perpendicular to the foliation, as are the [001] axes, the AV_{Smax} and V_{S1max} polarizations are vertical, V_{Pmin} is formed subparallel to the lineation, and the AV_{Smin} and V_{S1min} polarizations are subparallel to the lineation. The evaluated V_P, V_{S1}, and V_{S2} of average epidote are 7.09–7.75, 4.16–4.44, and 4.09–4.31 km/s, respectively (Fig. 9c). The seismic anisotropy of average epidote is relatively weak ($AV_P = 9.0\%$, $AV_S = 8.04\%$) compared with the other minerals. The patterns of seismic properties are similar to those of glaucophane, so that

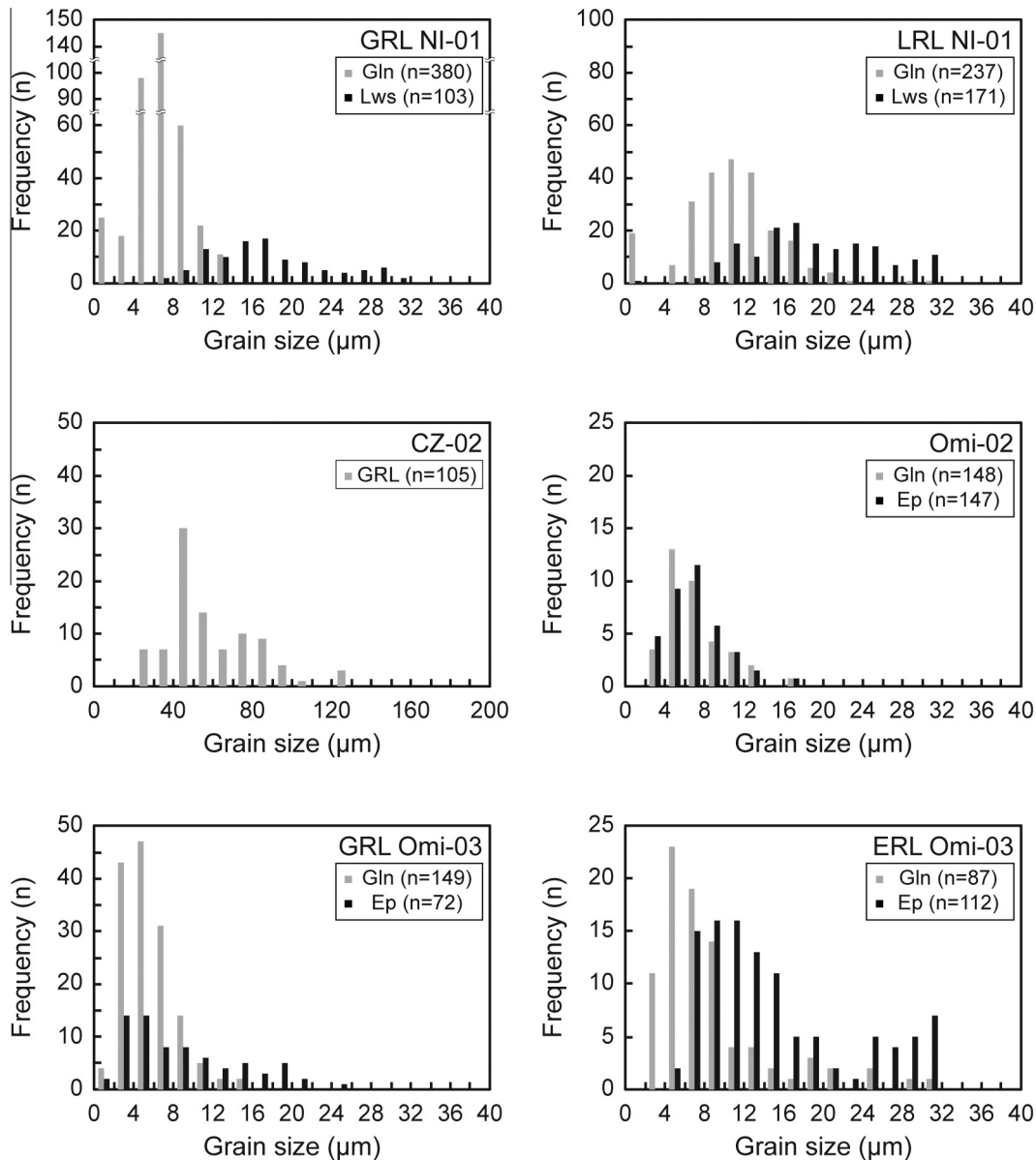**Fig. 5.** Grain size distributions. A square grain shape was assumed for grain size calculations. See the text for details.

the V_{Pmax} and AV_{Smax} of epidote are parallel to the lineation and foliation, respectively, and V_{Pmin} and AV_{Smin} are developed normal to the foliation.

The seismic properties of whole rocks are evaluated with the assumption that the lawsonite and epidote blueschists only contain glaucophane, lawsonite, and epidote. The New Idria lawsonite blueschist (NI-01) calculated on the basis of the averages for glaucophane and lawsonite has values of 6.99–8.31 km/s for V_P, 4.36–4.74 km/s for V_{S1}, and 4.27–4.51 km/s for V_{S2}, with AV_P being 12.0–17.2% and AV_S being 5.6–9.2% (Fig. 10a and b). The anisotropic seismic patterns of lawsonite blueschist are similar to those of glaucophane, with V_{Pmax} parallel to the lineation, AV_{Smax} and V_{S1max} polarizations parallel to the foliation, and V_{Pmin} and AV_{Smin} perpendicular to the foliation. The V_P of the Omi epidote blueschist (Omi-03), calculated from the average glaucophane and epidote, is 6.88–8.38 km/s, V_{S1} is 4.20–4.83 km/s, V_{S2} is 4.16–4.53 km/s, and the seismic anisotropy is stronger (AV_P = 11.8–19.6% and AV_S = 8.4–11.1%) than in the lawsonite blueschist (Fig. 10c and d). The V_{Pmax} and AV_{Smax} of the epidote blueschist are parallel to the lineation

and foliation, respectively, while V_{Pmin} and AV_{Smin} are developed normal to the foliation.

6. Discussion

6.1. Deformational mechanisms of glaucophane, lawsonite, and epidote

Microstructures are affected by (i) progressive metamorphism where rock-forming minerals transform according to the progressively changing mineral stability fields, and (ii) the deformation of minerals, the manner of which changes with the mineral and the various prevailing conditions. Natural amphiboles can be subject to different deformation mechanisms such as cataclastic deformation, rigid-body rotation, and dynamic recrystallization (Cumbest et al., 1989; Ildefonse et al., 1990; Nyman et al., 1992; Siegesmund et al., 1994). Glaucophane, on the other hand, tends to deform predominantly by crystal plastic mechanisms via the
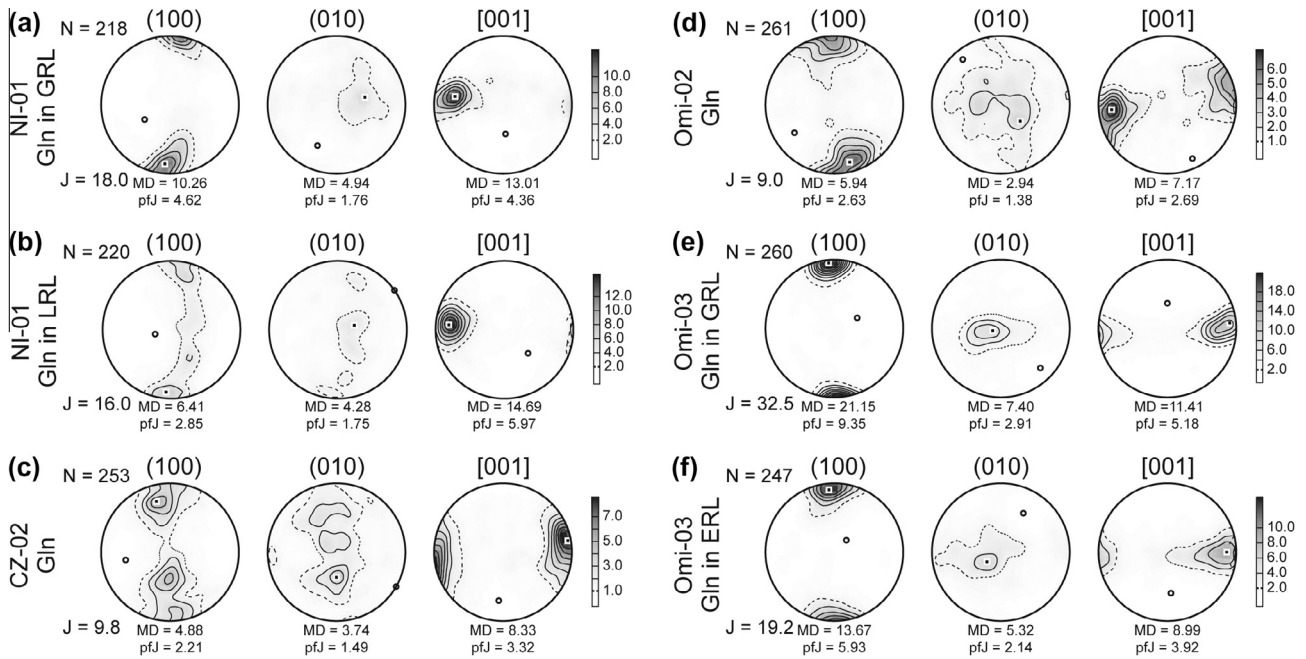
Fig. 6. Pole figures for glaucophane in the analyzed samples. Poles were plotted on lower hemisphere equal-area projections with contours in multiples of uniform distribution (m.u.d) for the density of poles. N: Number of measurements; J: J-index; MD: Maximum density.
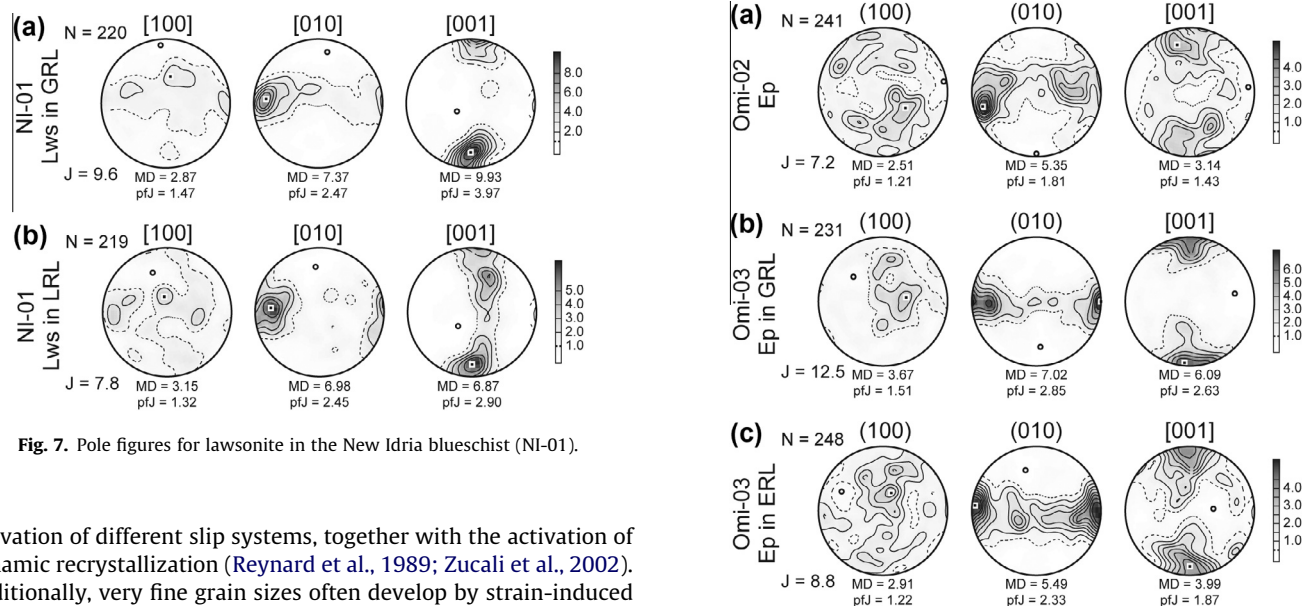

Fig. 7. Pole figures for lawsonite in the New Idria blueschist (NI-01).

Fig. 8. Pole figures for epidote in the Omi blueschists (Omi-02 and 03).

activation of different slip systems, together with the activation of dynamic recrystallization (Reynard et al., 1989; Zucali et al., 2002). Additionally, very fine grain sizes often develop by strain-induced recrystallization during or after crystal plastic deformation (e.g., Drury and Urai, 1990). In the present specimens, the glaucophanes display strong CPOs and a very fine grain size that is possibly the product of grain size reduction, suggesting that the microstructures formed as a result of dynamic recrystallization (e.g., Díaz Aspiroz et al., 2007). This interpretation is supported by the relationship between grain size and the J-index of pole figures, and by the presence of two peaks in the grain size distributions from some samples (Figs. 5 and 6; Table 1). Therefore, the glaucophanes exhibit characteristic of dynamic recrystallization, possibly accommodated by dislocation creep. The Omi garnet-bearing blueschists (Omi-02) exhibit gently curved grain boundaries between glaucophane and epidote, suggesting the activation of grain boundary area reduction during recovery (Fig. 2d). Irregular or curved grain boundaries of glaucophane imply annealing and grain growth as a result of the reduction of interfacial free energy in a low stress re-

gime (Fig. 2) (Evans et al., 2001). Although dissolution and precipitation creep are the dominant deformation mechanisms for calcic amphiboles at low temperatures, the weak chemical zoning and the very fine grain size of the analyzed glaucophanes demonstrate that these mechanisms were not important for the glaucophane.

On the other hand, the deformation mechanisms of lawsonite and epidote are poorly understood. Teyssier et al. (2010) interpreted lawsonite as a rigid phase based on the assumption that the associated glaucophane is weaker. Similarly, Kim et al. (2013) reported lawsonite to be stronger than glaucophane according to fabric analyses of two distinct layers in the New Idria lawsonite blueschist. Lawsonite in the present specimens has relatively
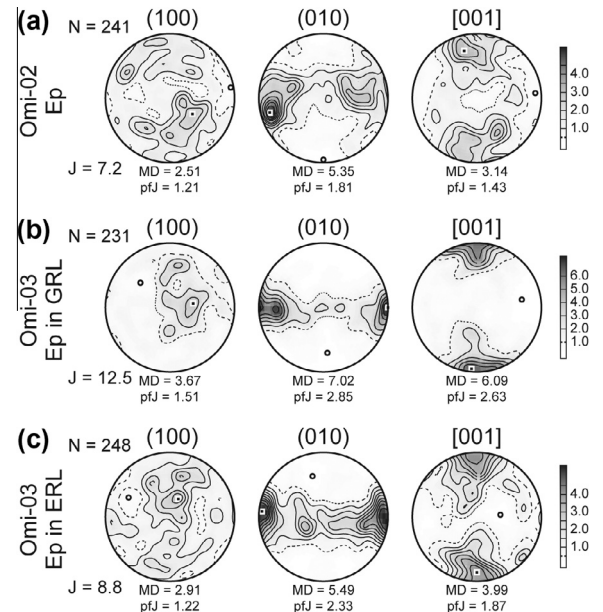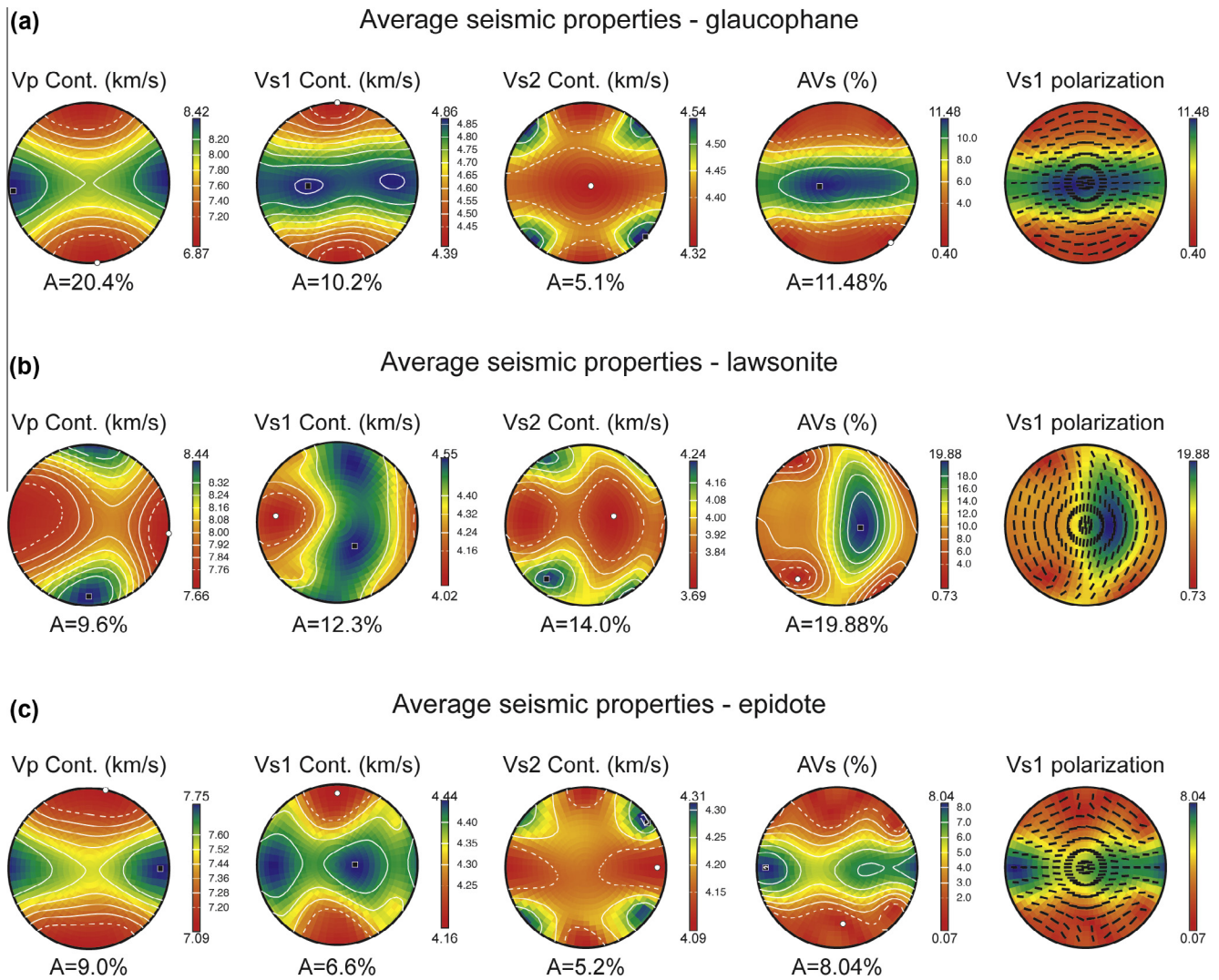
Fig. 9. Calculated seismic anisotropies of (a) average glaucophane, (b) lawsonite, and (c) epidote. The Voigt–Reuss–Hill averaging scheme and lower hemisphere equal area projections are used.

strong CPOs, even though euhedral grains are present with angular and straight boundaries (Fig. 2a and b). Therefore, the lawsonite microstructures that formed within the wide stability field of lawsonite possibly developed with the aid of rigid body rotations. Epidote in the present specimens also exhibits straight grain boundaries and euhedral shapes, implying rigid body rotation as the dominant deformation mechanism. In view of these straight grain boundaries, the two conspicuous grain-size-distribution peaks for epidote in the epidote-rich layer in Omi blueschist (ERL Omi-03) can probably be attributed to two stages of growth, during prograde and retrograde metamorphism, rather than to dynamic recrystallization (Figs. 2f and 5). Our results suggest, consequently, that microstructures of the bulk rock and each mineral such as epidote and lawsonite were decided by deformation of glaucophane.

6.2. P–T conditions of deformation

Lawsonite and epidote eclogites generally form at depths greater than 45 km in subduction zones (Tsujimori et al., 2006), and they transform to other minerals and rocks during the relatively low P–T conditions of exhumation so that they are relatively rare at the surface, especially without some degree of alteration. The Diablo Range and Ward Creek in California, and the Omi area in

central Japan, are unusual in that they expose unaltered lawsonite or epidote eclogites, implying rapid exhumation, probably as a result of slab breakoff. Lawsonite in the New Idria blueschist, and epidote in the Omi epidote blueschists, possibly formed during prograde subduction-related metamorphism, rather than during uplift and exhumation, based on the euhedral grain shapes and straight grain boundaries. At a late stage of subduction the maximum pressure conditions attained for the New Idria serpentinite body were >1.3 GPa (Tsujimori et al., 2007), and the maximum P–T conditions attained in the Hida metamorphic belt were >1.8 GPa and 550–600 °C (Tsujimori, 2002).

On the other hand, most of the glaucophane analyzed here possibly formed along a retrograde P–T path, based on its typical occurrence in the matrix, and the decrease in Al from core (glaucophane) to rim (winchite or actinolite). Although glaucophane in the glaucophane-rich layer in the Omi blueschist (GRL Omi-03) is the exception, in that it shows an increase of Al from core to rim, it still occurs in the matrix, and it might therefore have formed during retrogression and been altered after uplift. This can be supported by garnet-free assemblages of the Omi-03, in the retrograde P–T path of a previous study (Tsujimori, 2002). The well-aligned fabrics displayed by glaucophane, lawsonite, and epidote, characterized by the relatively low angles between crystal long axes and the mean
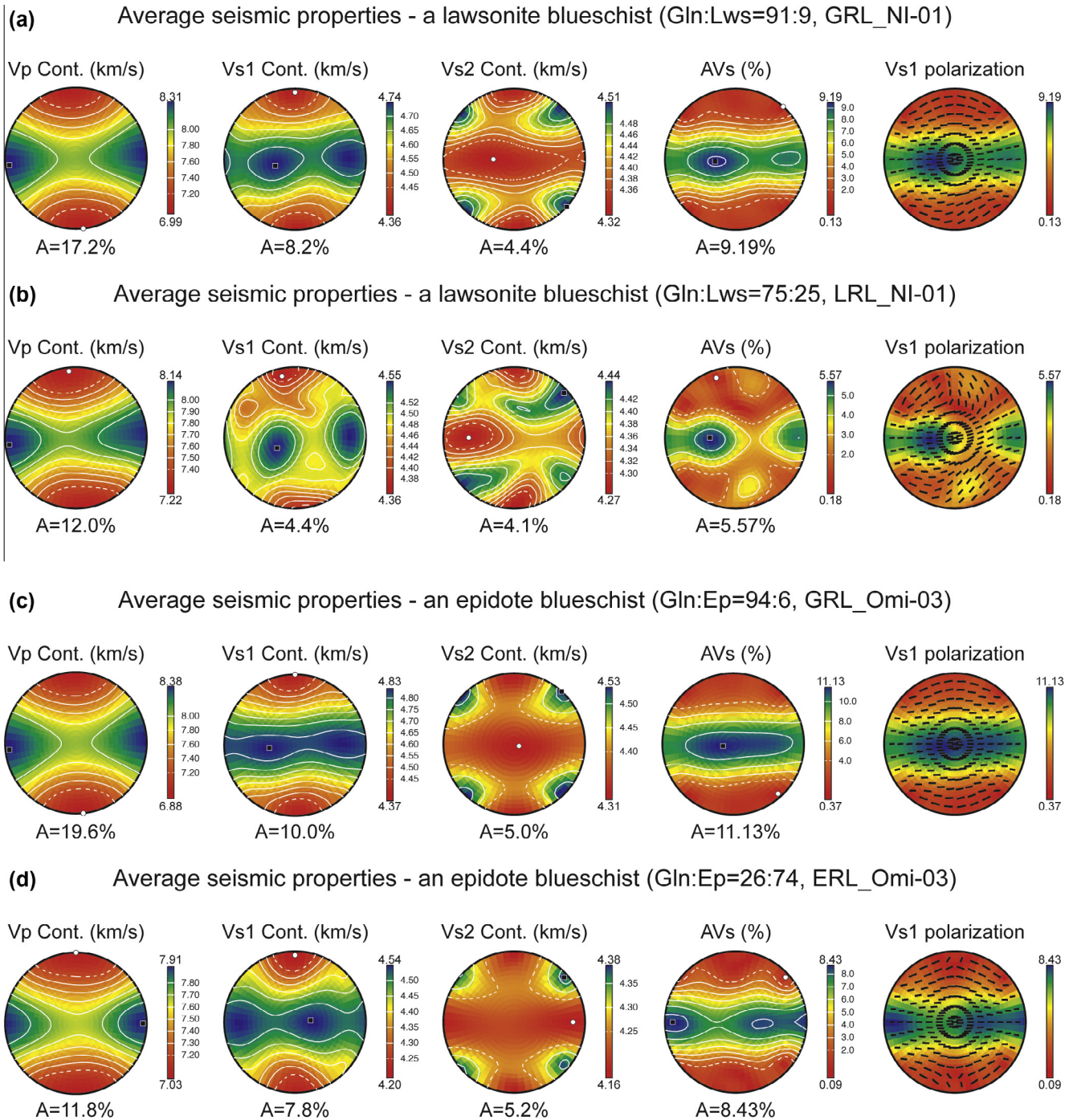
Fig. 10. Seismic anisotropy evaluated for lawsonite blueschists (a) GRL NI-01 and (b) LRL NI-01, and epidote blueschists (c) GRL Omi-03 and (d) LRL Omi-03.

position of the foliation plane, indicate that deformation took place during or after the blueschist-facies overprinting (Fig. 4). The strong CPOs that define the foliation might be attributed to the flow of dynamically recrystallized grains, denoting the presence of synkinematic microstructures (e.g., Hippertt and Hongn, 1998). Consequently, the microstructures in the analyzed samples are thought to have formed at $P > 1$ GPa and $T = 200$–$290\,°C$ for the New Idria blueschist (Tsujimori et al., 2007), $P = \sim1.8$–2.2 GPa and $T = 430$–$440\,°C$ for the Ward Creek blueschist (Tsujimori et al., 2006), and $P = \sim1$ GPa and $T = 400$–$460\,°C$ for the Omi blueschists (Tsujimori, 2002), consistent with the stability field of blueschist (Fig. 11).

6.3. Seismic properties of lawsonite and epidote blueschists in the subducting slab

The angle of subduction, which is influenced by the age of the crust and depositional materials during movement to the subduction zone, can affect the P–T increase during subduction; consequently, the geothermal gradient is high in SW Japan and low in NE Japan. Owing to the stability field of blueschist, lawsonite blueschist is the main constituent of the oceanic crust beneath NE Japan, while epidote blueschist is the main constituent beneath SW Japan. The V_P of lawsonite (6.99–8.31 km/s) and epidote blueschists (6.88–8.38 km/s), as modeled from the average seismic
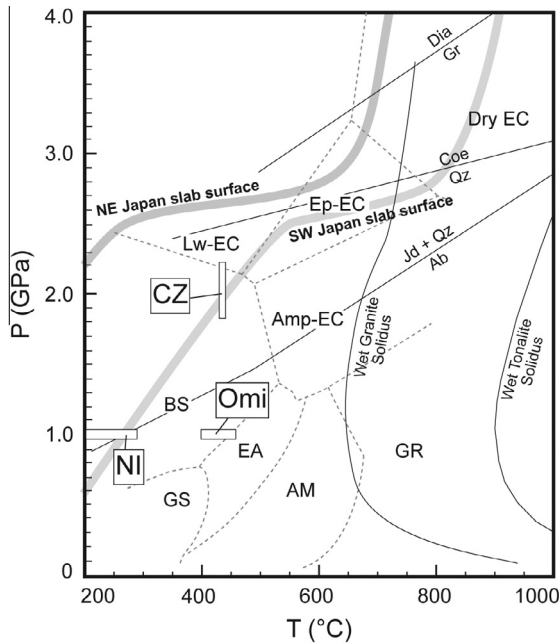
Fig. 11. Deformational *P–T* conditions for the analyzed samples. The pressure–temperature paths for NE and SW Japan are after Syracuse et al. (2010). GS: greenschist; AM: amphibolite; EA: epidote amphibolite; GR: granulite; BS: blueschist; Amp-EC: amphibole eclogite; Lw-EC: lawsonite eclogite; Ep-EC: epidote eclogite; Dry EC: dry eclogite; NI: NI-01; CZ: CZ-02; Omi: Omi-02 and 03.


Fig. 12. A graph for AV_{Pmax} and AV_{Smax} according to modal abundance. The AV_{Pmax} and AV_{Smax} of blueschists were computed from the average of the seismic anisotropies of glaucophane and lawsonite with every 10% step.

properties of their main rock-forming minerals, are higher than the values at ~30–50 km depth derived from recent seismological studies in NE Japan (7.1–7.4 km/s; Tsuji et al., 2008) and SW Japan (7.1–7.5 km/s; Shelly et al., 2006) (Fig. 10). The slightly faster seismic velocity in SW Japan, compared with NE Japan, is consistent, however, with our study. The average velocities of lawsonite blueschist are V_P = 7.67 km/s and V_S = 4.44 km/s (Fig. 10a and b), and these are similar values to the modeled result of V_P = 7.71 km/s and V_S = 4.49 km/s (Bezacier et al., 2010), as well as an experimental result of V_P = 6.0–7.4 km/s (Fujimoto et al., 2010). Therefore, since the seismic properties calculated for our samples are similar to those previously observed and modeled, and to experimental data, it suggests that our results are valid for the purposes of our study.

To better understand the implications of the seismic anisotropy of bulk rock masses, the AV_{Pmax} and AV_{Smax} of lawsonite and epidote blueschists have been computed using the assumption that a mass of rock is composed mainly of diverse modal abundances of average glaucophane, lawsonite, and epidote (Fig. 12). The seismic anisotropy of lawsonite blueschist is evaluated as AV_P = 3.9–20.4% and AV_S = 4.54–19.88% with a 'concave' feature characterized by lower values in the center and higher values in both ends (Fig. 12). An offset of the different propagating directions of seismic waves between glaucophane and lawsonite may cause the specific 'concave' feature, which is distinct from the 'straight' (directly or inversely proportional) change of AV_P and AV_S that is attributed to the same propagating direction of seismic waves in glaucophane and epidote (Bezacier et al., 2010; Satsukawa et al., 2011). The AV_P and AV_S of epidote blueschist are calculated as AV_P = 9.0–20.4 km/s and AV_P = 8.04–11.48 km/s with 'straight' lines. Consequently, we note that the seismic anisotropy of a mass of rock, especially one composed of highly anisotropic phases, is controlled by the modes of the constituent rock-forming minerals and the anisotropic seismic patterns of each phase. This proposition is consistent with the stronger trench-parallel seismic anisotropy in the Ryukyu arc (epidote blueschist) and the weaker anisotropy in NE Japan (lawsonite
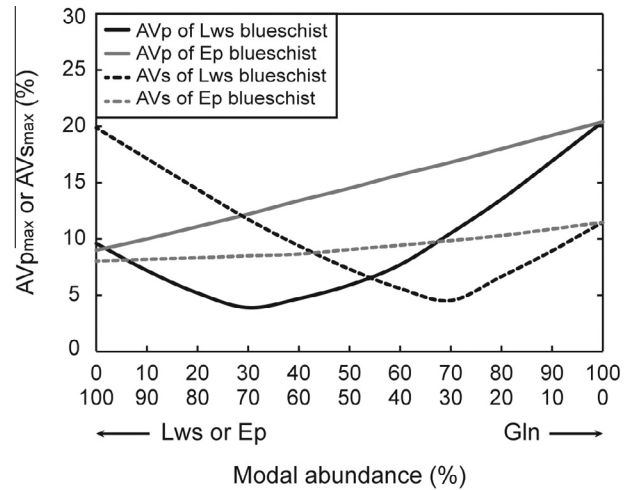
blueschist). The fastest V_P and AV_S of glaucophane and bulk rocks are along the foliation, whereas V_{Pmin} and AV_{Smin} are developed normal to the foliation and lineation (Figs. 9a and 10). The results indicate that a weak seismic anisotropy develops subnormal to the shear direction, and also that the V_{Pmax} and AV_{Smax} of glaucophane and the bulk rock are subparallel to the movement direction. Deformation mainly occurs in response to the movement direction of the subducting plate, and the fast shear wave is therefore established subparallel to the trench (trench-parallel fast anisotropy) (Fig. 13). On the other hand, lineation-perpendicular propagations of the fast V_{S1} polarization of lawsonite are generated perpendicular to the movement direction of the subducting oceanic crust, and hence a trench-perpendicular anisotropy can occur (Fig. 13).

The strong anisotropic properties of minerals can also be useful for understanding the nature of the LVL (Nikulin et al., 2009; Bostock, 2012; Wirth and Long, 2012). Chantel et al. (2012) reported a reasonably low V_S of lawsonite with strong anisotropy due to the (0 1 0)[0 0 1] slip system, which is in contrast to other studies (Fujimoto et al., 2010; Teyssier et al., 2010), including the present study. We therefore apply the results of our study to the LVL according to subducting angles, mainly using the preferred orientations and V_P/V_S ratios of minerals. A low seismic velocity can be produced when seismic waves propagate along the V_{Pmin} and V_{Smin} directions of minerals. For local events, slow seismic waves can be generated by changes in rock type, such as eclogite to blueschist, and the V_{Pmin} and V_{Smin} therefore need to be parallel to the lineation in the eclogite. This explains why the [0 1 0] axes of lawsonite are more appropriate rather than the (0 1 0) planes of epidote for local events. On the other hand, teleseismic waves can be generated normal to the surface of the crust, and this is suitable for a warm slab in which the (1 0 0) planes of glaucophane contain V_{Pmin} and V_{Smin}. The V_P/V_S ratios are calculated as 2.08 for lawsonite (V_P = 7.66 km/s and V_S = 3.69 km/s) and 1.59 for glaucophane (V_P = 6.87 km/s and V_S = 4.32 km/s). Although the V_P/V_S ratios estimated for glaucophane are rather low, the values for lawsonite are higher than those for the other minerals present. Therefore, lawsonite might contribute to the low velocity layer with high V_P/V_S ratios, whereas blueschists lacking lawsonite require other minerals such as serpentine or pore fluids along the grain-boundaries.

The thickness of an anisotropic layer is used to compare the seismic properties of glaucophane, lawsonite, and epidote with other well-known anisotropic minerals such as olivine and serpentine (e.g., Katayama, 2009). The thickness (D) of the anisotropic
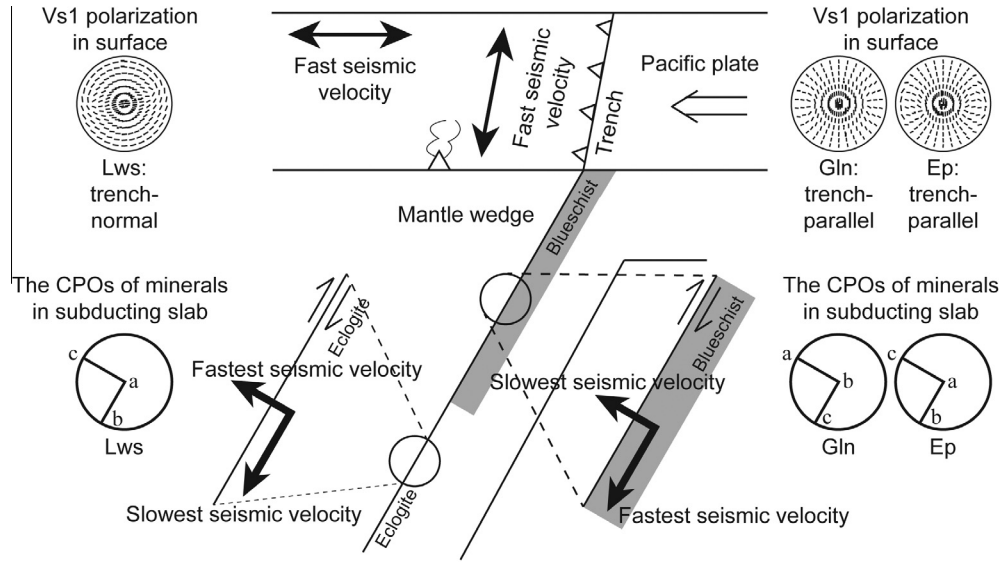
Fig. 13. A schematic model showing trench-parallel and trench-normal fast anisotropies. The subducting angle is assumed to be 60°, however the patterns of V_{s1} polarization at the surface is based on 90° of subducting angle.

layer is decided by the multiplication of velocity (v) and time (t), and hence the delay time (dt) is defined by the following equation:

$$dt = AV_S / < V_S > D,$$

where AV_S is the anisotropy of a specific propagation direction and $<V_S>$ indicates the average velocity of the fast and slow velocities. Fig. 14 shows the relations between the delay time and the thickness of the seismically anisotropic layer that is composed of glauco-phane, lawsonite, and epidote aggregates. The calculated results for olivine ($AV_S = 4.5\%$ and $<V_S> = 4.75$ km/s; Katayama and Karato, 2006) and serpentine ($AV_S = 36.0\%$ and $<V_S> = 4.13$ km/s; Katayama et al., 2009) are shown for comparison. With respect to the observed delay time (0.06–0.10 s) of trench-parallel AV_S beneath NE Japan (Nakajima and Hasegawa, 2004), the thickness of the anisotropic layer is calculated to be 2–4 km for average glaucophane, and 3–4 km for average epidote (Fig. 14). The estimates are thicker than the calculated thickness for serpentine (1 km), but noticeably thinner than for olivine (6–11 km). Using a 7 ± 1 km thickness for the oceanic crust (White et al., 1992), a 2–4 km anisotropic layer caused by glaucophane is capable of producing the trench-parallel fast anisotropy beneath NE Japan (cold subducting slab). On the other hand, the thickness of the anisotropic layer caused by lawsonite is calculated to be 2–5 km for trench-normal fast anisotropy, based on the observed delay times (0.10–0.26 s) in NE Japan (Nakajima and Hasegawa, 2004). Given the delay time ($\sim$1–2 s) beneath the Ryukyu arc (Long and van der Hilst, 2005), the thickness can be computed to be 39–79 km for average glaucophane and 42–83 km for average epidote (Fig. 14). The thickness of an anisotropic layer comprising serpentine (11–23 km) or olivine (105–211 km) is insuf-ficient to explain the strong seismic anisotropy beneath the Ryukyu arc (hot subducting slab) only by a single mineral phase. Our results suggest, therefore, that beneath NE Japan, glaucophane may con-tribute to the trench-parallel seismic anisotropy in the forearc, and lawsonite to the trench-normal anisotropy in the back-arc. Be-neath the Ryukyu arc, serpentine and olivine may also partly help to generate the seismic anisotropy.

Natural rocks, however, are composed of poly-phases, and the mineral assemblages need to be considered along with the subduc-tion processes. The lawsonite blueschists contain 75–91% of glau-cophane and 9–25% of lawsonite, and these main constituents show different seismic anisotropic patterns from each other
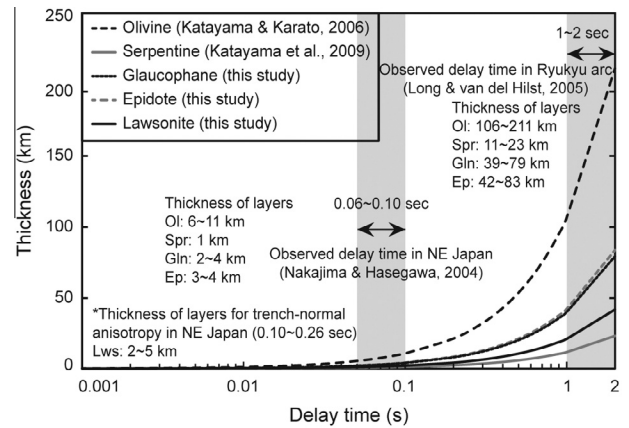
Fig. 14. Relationship between the calculated thickness of the anisotropic layer and the delay time. The delay time and thickness of an anisotropic layer of olivine ($AV_S = 4.5\%$, $<V_S> = 4.75$ km/s; Katayama and Karato, 2006) and serpentine ($AV_S = 35.9\%$, $<V_S> = 4.13$ km/s; Katayama et al., 2009) are also plotted for comparison.

(Fig. 10a, b; Table 1). On the other hand, the epidote blueschists consist mainly of glaucophane 26–94% and epidote 6–74%, and these minerals have similar anisotropic patterns (Fig. 10c, d; Ta-ble 1). The similar anisotropic patterns of epidote and glaucophane lead one to suggest that the seismic anisotropy of epidote blue-schist is the same as the average values of the epidote and glauco-phane seismic anisotropies (Figs. 9a, c and 10). The differing patterns of seismic anisotropy for lawsonite and glaucophane, however, act against each other, so that a lawsonite blueschist has a lower seismic anisotropy than an epidote blueschist (Figs. 9a, b and 12). The countervailing effect of lawsonite might be related to the weak trench-parallel seismic anisotropy in NE Ja-pan, whereas the complementary patterns of the seismic anisotro-pies of epidote and glaucophane might be the cause of the strong trench-parallel seismic anisotropy in the Ryukyu arc. Beneath NE Japan, glaucophane, along with the countervailing effects of laws-onite, controls the seismic anisotropy of the subducting slab at $\sim$30–110 km depth. At 110 km depth the glaucophane breaks down, and omphacite forms within the stability field of lawsonite

during eclogitization. The seismic anisotropy of eclogite may be governed, therefore, by a strongly seismic anisotropic mineral such as lawsonite (AV_P = 9.6% and AV_S = 19.88% in our samples), because the seismic anisotropy of omphacite is low (AV_{Pmax} = 1.9%, AV_{Smax} = 2.5%; Bascou et al., 2001). In addition, lawsonite has a V_{S1} polarization that is perpendicular to the foliation, and this can explain the trench-perpendicular seismic anisotropy observed beneath NE Japan. Other factors, such as physical variables or microstructural conditions (minor phases, grain boundaries, microcracks, and alteration), need to be considered for a complete understanding of seismic velocities, but the above results suggest that trench-parallel and trench-normal seismic anisotropy beneath NE Japan can be explained by glaucophane and lawsonite, respectively, and that the weak trench-parallel anisotropy beneath NE Japan can be attributed to the countervailing effects of lawsonite. In addition, the strong seismic anisotropy beneath the Ryukyu arc might be dominated in the subducting oceanic crust by combinations of minerals with similar seismic anisotropic patterns, such as glaucophane and epidote, and in the mantle wedge by minerals such as serpentine and olivine.

7. Conclusions

We presented important new data concerning (i) the seismic anisotropy of subducting oceanic crust and (ii) the microstructures and deformational behavior of rock-forming minerals in natural lawsonite blueschists from the Diablo Range and the Franciscan Complex in California, and in natural epidote blueschists from the Hida Mountains, Japan. We carefully compared the calculated seismic velocities and anisotropies of glaucophane, lawsonite, and epidote with observatory data for subduction zones. The principal results of our investigations into the microstructures and seismic properties are as follows.

(1) Glaucophane, as the main constituent of the matrix, is very fine grained, has a strong shape preferred orientations, high aspect ratios, and distinct CPOs (Figs. 1, 2, 4 and 6). All microstructures of the glaucophane suggest *characteristic of dynamic recrystallization probably activated by dislocation creep*. On the other hand, lawsonite and epidote both occur as porphyroclasts, and their euhedral grain shapes and straight grain boundaries (Figs. 1, 2, 4, 7 and 8) indicate that deformation took place primarily by rigid body rotation.

(2) The calculated average seismic velocities (V_P = 6.87–8.42 km/s, V_S = 4.32–4.86 km/s for glaucophane; V_P = 7.66–8.44 km/s, V_S = 3.69–4.55 km/s for lawsonite; V_P = 7.09–7.75 km/s, V_S = 4.09–4.44 km/s for epidote) are similar to previous observations (Shelly et al., 2006; Tsuji et al., 2008), modeling results (Bezacier et al., 2010), and experimental data (Fujimoto et al., 2010) (Fig. 9). For an average glaucophane and epidote, the propagations of V_P and V_S polarization develop along the lineation and foliation, respectively, while for an average lawsonite they are subnormal to the foliation and lineation, respectively. Foliation-subparallel V_S polarization in glaucophane and epidote can generate a trench-parallel seismic anisotropy owing to the development of a foliation parallel to the direction of the subduction, whereas the V_S polarization of lawsonite can establish a trench-normal seismic anisotropy (Fig. 13).

(3) Relatively strong seismic anisotropies were calculated for the main mineral phases in blueschists (AV_P = 20.4%, AV_S = 11.5% for glaucophane; AV_P = 9.6%, AV_S = 19.9% for lawsonite; AV_P = 9.0%, AV_S = 8.0% for epidote) (Fig. 9). A thin anisotropic layer composed of glaucophane, epidote, and lawsonite is sufficient to explain the observed delay time

of trench-parallel (0.06–0.10 s) and trench-normal (0.10–0.26 s) shear wave splitting beneath NE Japan (Nakajima and Hasegawa, 2004), but it is insufficient for the Ryukyu arc (1–2 s; Long and van der Hilst, 2005) (Fig. 14). The calculations based on the relative abundance of the constituent minerals are consistent with the 'concave' changes of AV_P and AV_S that depend on mineral abundances, and also with the stronger trench-parallel anisotropy in the Ryukyu arc and the weaker seismic anisotropy in NE Japan (Fig. 12). All the data collected from natural blueschists indicate the seismic anisotropies of lawsonite and epidote, in combination with that of glaucophane, play important roles in producing the trench-parallel and trench-normal seismic anisotropies, and they also provide explanations for the low velocity layer in subduction zones.

References

Aleksandrov, K.S., Alchikov, U.V., Belikov, B.P., Zaslavskii, B.I., Krupnyi, A.I., 1974. Velocities of elastic waves in minerals at atmospheric pressure and increasing precision of elastic constants by mean of EVM (in Russian). Izv. Acad. Sci. USSR Seol. Ser. 10, 15–24.

Banno, S., 1958. Glaucophane schists and associated rocks in the Omi district, Niigata Prefecture, Japan. Jpn. J. Geol. Geogr. 29, 29–44.

Bascou, J., Barruola, G., Vaucheza, A., Mainprice, D., Egydio-Silva, M., 2001. EBSD-measured lattice-preferred orientations and seismic properties of eclogites. Tectonophysics 342, 61–80.

Bezacier, L., Reynard, B., Bass, J.D., Wang, J., Mainprice, D., 2010. Elasticity of glaucophane, seismic velocities and anisotropy of the subducted oceanic crust. Tectonophysics 494, 201–210.

Bostock, M.G., 2012. The Moho in subduction zones. Tectonophysics, in press. http://dx.doi.org/10.1016/j.tecto.2012.07.007.

Bunge, H.J., 1982. Texture Analysis in Materials Science. Butterworth, London, p. 559.

Chantel, J., Mookherjee, M., Frost, D.J., 2012. The elasticity of lawsonite at high pressure and the origin of low velocity layers in subduction zones. Earth Planet. Sci. Lett. 349–350, 116–125.

Coleman, R.G., 1980. Tectonic inclusions in serpentinite. Arch. Sci. Société de Physique et d'Histoire Naturelle de Genève 33, 89–102.

Coleman, R.G., Lee, D.E., 1963. Ultrahigh-Pressure Metamorphism. Cambridge University Press, New York, pp. 528.

Cumbest, R.J., Drury, M.R., Van Roermund, H.L.M., Simpson, C., 1989. Dynamic recrystallization and chemical evolution of clinoamphibole from Senja Norway. Contrib. Mineral. Petrol. 101, 339–349.

Deer, W.A., Howie, R.A., Zussman, J., 1992. The Rock-forming Minerals, second ed. Longmans, London, p. 266.

Díaz Aspiroz, M., Lloyd, G.E., Fernández, C., 2007. Development of lattice preferred orientation in clinoamphiboles deformed under low-pressure metamorphic conditions. A SEM/EBSD study of metabasites from the Aracena metamorphic belt (SW Spain). J. Struct. Geol. 29, 629–645.

Drury, M.R., Urai, J.L., 1990. Deformation-related recrystallization processes. Tectonophysics 172, 235–253.

Evans, B., Renner, J., Hirth, G., 2001. A few remarks on the kinetics of static grain growth in rocks. Int. J. Earth Sci. 90, 88–103.

Fujimoto, Y., Kono, Y., Hirajima, T., Kanagawa, K., Ishikawa, M., Arima, M., 2010. P-wave velocity and anisotropy of lawsonite and epidote blueschists: constraints on water transportation along subducting oceanic crust. Phys. Earth Planet. Inter. 183, 219–228.

Hippertt, J.F., Hongn, F.D., 1998. Deformation mechanisms in the mylonite/ultramylonite transition. J. Struct. Geol. 20, 1435–1448.

Ildefonse, B., Lardeauz, J.-M., Caron, J.-M., 1990. The behavior of shape preferred orientations in metamorphic rocks: amphiboles and jadeites from the Monte Mucrone area (Sesia–Lanzo zone, Italian Western Alps). J. Struct. Geol. 12, 1005–1011.

Jung, H., Karato, S.-I., 2001. Water-induced fabric transitions in olivine. Science 293, 1460–1463.

Katayama, I., 2009. Thin anisotropic layer in the mantle wedge beneath northeast Japan. Geology 37, 211–214.

Katayama, I., Karato, S.-I., 2006. Effect of temperature on the B- to C-type olivine fabric transition and implication for flow pattern in the subduction zone. Phys. Earth Planet. Inter. 157, 33–45.

Katayama, I., Hirauchi, K., Michibayashi, K., Ando, J., 2009. Trench-parallel anisotropy produced by serpentine deformation in the hydrated mantle wedge. Nature 461, 1114–1117.

Kim, D., Katayama, I., Michibayashi, K., Tsujimori, T., 2013. Rheological contrast between glaucophane and lawsonite in naturally deformed blueschist from Diablo Range, California. Isl. Arc 22, 63–73. http://dx.doi.org/10.1111/iar.12003.

Kita, S., Okada, T., Nakajima, J., Matsuzawa, T., Hasegawa, A., 2006. Existence of a seismic belt in the upper plane of the double seismic zone extending in the along-arc direction at depths of 70–100 km beneath NE Japan. Geophys. Res. Lett. 33, L24310.

Leake, B.E., Woolley, A.R., Arps, C.E.S., Birch, W.D., Gilbert, M.C., Grice, J.D., Hawthorne, F.D., Kato, A., Kisch, H.J., Krivovichev, V.G., Linthout, K., Laird, J., Mandarino, J.A., Maresch, W.V., Nickel, E.H., Rock, N.M.S., Schumacher, J.C., Smith, D.C., Stephenson, N.C.N., Ungaretti, L., Whittaker, E.J.W., Youzhi, G., 1997. Nomenclature of amphiboles: report of the subcommittee on amphiboles of the international mineralogical association, commission on new minerals and mineral names. Can. Mineral. 35, 219–246.

Long, D.L., van der Hilst, R.D., 2005. Upper mantle anisotropy beneath Japan from shear wave splitting. Phys. Earth Planet. Inter. 151, 206–222.

Long, M.D., Silver, P.G., 2008. The subduction zone flow field from seismic anisotropy: A global view. Science 18, 315–318.

Mainprice, D., 1990. An efficient Fortran program to calculate seismic anisotropy from the lattice preferred orientation of minerals. Comput. Geosci. 16, 385–393.

Mainprice, D., Silver, P.G., 1993. Interpretation of SKS-waves using samples from the subcontinental lithosphere. Phys. Earth Planet. Inter. 78, 257–280.

Mainprice, D., Barruol, G., Ben Ismaïl, W., 2000. The anisotropy of the Earth's mantle: from single crystal to polycrystal. In: Karato, S., Forte, A.M., Liebermann, R.C., Masters, G., Stixrude, L. (Eds.), Mineral Physics and Seismic Tomography: From Atomic to Global, Geoph. Monog., vol. 117. pp. 237–264.

Mao, Z., Jiang, F., Duffy, T.S., 2007. Single-crystal elasticity of zoisite $Ca_2Al_3Si_3O_{12}$ (OH) by Brillouin scattering. Am. Mineral. 92, 570–576.

Maruyama, S., Cho, M., Liou, J.G., 1986. Experimental investigations of blueschist–greenschist transition equilibria: pressure dependence of Al_2O_3 contents in sodic amphiboles—A new barometer. In: Evans, B.W., Brown, E.H. (Eds.), Blueschist and Eclogite, Geol. Soc. Am. Mem., vol. 164. pp. 1–16.

Maruyama, S., Liou, J.G., 1987. Clinopyroxene a mineral telescoped through the processes of blueschist facies metamorphism. J. Metamorph. Geol. 5, 529–552.

Maruyama, S., Liou, J.G., 1988. Petrology of Franciscan metabasites along the jadeite–glaucophane type facies series, Cazadero, California. J. Petrol. 29, 1–37.

Mezger, J.E., 2010. Rotation of irregular staurolite porphyroblasts in a simple shear dominated shear zone controlled by initial growth orientation and aspect ratio. J. Struct. Geol. 32, 1147–1157.

Mookherjee, M., Bezacier, L., 2012. The low velocity layer in subduction zone: structure and elasticity of glaucophane at high pressures. Phys. Earth Planet. Inter. 208–209, 50–58.

Nakajima, J., Hasegawa, A., 2004. Shear-wave polarization anisotropy and subduction induced flow in the mantle wedge of northeastern Japan. Earth Planet. Sci. Lett. 225, 365–377.

Nikulin, A., Levin, V., Park, J., 2009. Receiver function study of the Cascadia megathrust: evidence for localized serpentinization. Geochem. Geophys. Geosyst. 10, Q07004.

Nyman, M.W., Law, R.D., Smelik, E., 1992. Cataclastic deformation for the development of core mantle structures in amphibole. Geology 20, 455–458.

Prior, D.J., Boyle, A.P., Brenker, F., Cheadle, M.C., Day, A., Lopez, G., Peruzzo, L., Potts, G.J., Reddy, S., Spiess, R., Timms, N.E., Trimby, P., Wheeler, J., Zetterstrom, L., 1999. The application of electron backscatter diffraction and orientation contrast imaging in the SEM to textural problems in rocks. Am. Mineral. 84, 1741–1759.

Randle, V., 1992. Microtexture Determination and its Applications. The Institute of Materials, Minerals and Mining, London, p. 174.

Randle, V., Engler, O., 2000. Introduction to Texture Analysis: Macrotexture, Microtexture and Orientation Mapping. CRC Press, London, p. 408.

Reynard, B., Gillet, P., Willaime, C., 1989. Deformation mechanisms in naturally deformed glaucophanes: a TEM and HREM study. Eur. J. Mineral. 1, 611–624.

Satsukawa, T., Michibayashi, K., Anthony, E.Y., Stern, R.J., Gao, S.S., Liu, K.H., 2011. Seismic anisotropy of the uppermost mantle beneath the Rio Grande rift: evidence from Kilbourne Hole peridotite xenoliths, New Mexico. Earth Planet. Sci. Lett. 311, 172–181.

Schmidt, M.W., Poli, S., 1998. Experimentally based water budgets for dehydrating slab and consequences for arc magma generation. Earth Planet. Sci. Lett. 163, 361–379.

Shelly, D.R., Beroza, G.C., Ide, S., Nakamura, S., 2006. Low-frequency earthquake in Shikoku, Japan, and their relationship to episodic tremor and slip. Nature 422, 188–191.

Siegesmund, S., Helming, K., Kruse, R., 1994. Complete texture analysis of a deformed amphibolite: comparison between neutron, diffraction and U-stage data. J. Struct. Geol. 16, 131–142.

Sinogeikin, S.V., Schilling, F.R., Bass, J.D., 2000. Single crystal elasticity of lawsonite. Am. Mineral. 85, 1834–1837.

Syracuse, E.M., van Keken, P.E., Abers, G.A., 2010. The global range of subduction zone thermal models. Phys. Earth Planet. Inter. 183, 73–90.

Teyssier, C., Whitney, D.L., Toraman, E., Seaton, N.C.A., 2010. Lawsonite vorticity and subduction kinematics. Geology 38, 1123–1126.

Tsuji, Y., Nakajima, J., Hasegawa, A., 2008. Tomographic evidence for hydrated oceanic crust of the Pacific slab beneath northeastern Japan: implications for water transportation in subduction zones. Geophys. Res. Lett. 35, L14308.

Tsujimori, T., 2002. Prograde and retrograde P–T paths of the Late Paleozoic glaucophane eclogite from the Renge Metamorphic Belt, Hida Mountains, Southwestern Japan. Int. Geol. Rev. 44, 797–818.

Tsujimori, T., Ishiwatari, A., Banno, S., 2000. Eclogitic glaucophane schist from the Yunotani valley in Omi Town, the Renge metamorphic belt, the Inner Zone of southwestern Japan. J. Geol. Soc. Jpn. 106, 353–362 (in Japanese with English abstract).

Tsujimori, T., Sisson, V.B., Liou, J.G., Harlow, G.E., Sorensen, S.S., 2006. Very-low-temperature record in subduction process: a review of worldwide lawsonite eclogites. Lithos 92, 609–624.

Tsujimori, T., Liou, G.J., Coleman, R.G., 2007. Finding of high-grade tectonic blocks from the New Idria serpentinite body, Diablo Range, California: petrologic constraints on the tectonic evolution of an active serpentinite diapir. In: Cloos, M., Carlson, W.D., Gilbert, M.C., Liou, J.G., Sorensen, S.S. (Eds.), Convergent Margin Terranes and Associated Regions: a Tribute to Ernst, W.G., Geol. S. Am. S., vol. 419. pp. 67–80.

White, R.S., McKenzie, D., O'Nions, R.K., 1992. Oceanic crustal thickness from seismic measurements and rare earth element inversions. J. Geophys. Res. 97, 19683–19715.

Whitney, D.L., Evans, B.W., 2010. Abbreviations for names of rock-forming minerals. Am. Mineral. 95, 185–187.

Wines, D.A., Conder, J.A., Faul, U.J., 2008. The seismic structure and dynamics of the mantle wedge. Annu. Rev. Earth Planet. Sci. 36, 421–455.

Wirth, E.A., Long, M.D., 2012. Multiple layers of seismic anisotropy and a low-velocity region in the mantle wedge beneath Japan: evidence from teleseismic receiver functions. Geochem. Geophys. Geosyst. 13, Q08005.

Zucali, M., Chateigner, D., Dugnani, M., Lutterotti, L., Ouladdiaf, B., 2002. Quantitative texture analysis of glaucophanite deformed under eclogite facies conditions (Sesia–Lanzo Zone, Western Alps): comparison between X-ray and neutron diffraction analysis. Geol. Soc. Lond. Spec. Publ. 200, 239–253.